RSC Advances

PAPER

View Article Online
View Journal | View Issue

Cite this: *RSC Adv.*, 2025, **15**, 33456

Tough dual-network Janus hydrogel patch for universal and reversible adhesion

Xiuli Pu,[a] Buyun Chen,[a] Qiang Li,[a] Chen Chen*[b] and Xinling Wang *[a]

Received 9th June 2025
Accepted 19th August 2025

DOI: 10.1039/d5ra04058b

rsc.li/rsc-advances

Traditional hydrogel adhesives hold tremendous potential in applications of hemostasis, wound closure, and tissue regeneration. However, significant challenges exist concerning the unsatisfactory mechanical properties and indiscriminate adhesion of the hydrogel, which possibly result in unwanted postoperative adhesion of tissues. In this work, a Janus hydrogel was fabricated from naturally-derived aspartic acid, glutamic acid, and dopamine. The hydrogel accomplishes the dual-sided property modulation through the coordination of Fe^{3+}, maintaining high adhesion on one side while eliminating most of the adhesion on the other, efficiently averting unintended adhesion. Remarkably, this hydrogel patch not only attained robust mechanical strength (around 410 kPa) and stability *via* the formation of a secondary network through coordination bonds, but also exhibited excellent adhesion properties (over 550 J m^{-2}) and repeatable adhesion (less than 20% decreasing after 5 adhesion cycles) originating from catechol surface chemistry and topological entanglement strategies. Moreover, the hydrogel boasts exceptional biocompatibility, making it advantageous for diverse biomedical scenarios.

1. Introduction

Hydrogel adhesives have demonstrated significant potential in biomedical applications such as hemostasis materials, wound closure, and tissue regeneration,[1–5] owing to their flexibility, biocompatibility, tissue resemblance and inherent nature of maintaining a moist environment. Hydrogel patches, as a type of hydrogel adhesive, are thin-sheet devices fabricated from hydrogel material, designed for adhesion to the skin or other tissue surfaces, and significantly enhance the convenience of practical applications due to their pre-formability.[6–8] For clinical cardiac repair, Peier *et al.* engineered a conductive and wet-adhesive hydrogel-based cardiac patch by integrating polyphenol-derived redox-active and conductive nanoparticles within a flexible gelatin network.[9] These patches require a brief contact for only several seconds to achieve strong and lasting adhesion effects.[10] However, these traditional hydrogel adhesives still have some shortcomings. Hyaluronic acid (HA)-based hydrogels adhesives were commonly used because of their good biocompatibility, but their applications were constrained because they are prone to deform and break when subjected to external forces due to the relatively low tensile strength and elastic modulus and the intrinsic feature that they are degraded rapidly *in vitro*.[11] Besides, undesired secondary adhesion caused by the two-sided adhesive nature,[12,13] which will compromise the material's functionality by facilitating inadvertent contamination of the non-wound-facing surface, is also a fatal weakness.[14] More severely, this indiscriminate adhesion usually resulted in adhesion to another side tissue, thereby impairing wound healing processes.[15]

To solve these issues, researchers have turned to Janus hydrogel patches with asymmetric structures and adhesion properties.[16,17] For example, Peng *et al.* reported a three-layer biodegradable Janus tissue patch that enables efficient closure of bleeding wounds and suppressed postoperative adhesion of tissues by multilayered composite processing.[18] Besides, suitable mechanical properties and good biocompatibility are also required for long-term use of hydrogel patches in complex physicochemical environments. To enhance their performance, the introduction of a secondary network structure by the coordination of metal ions and functional groups of polymer chains is considered a good choice to strengthen the stability of the polymer network.[19–21] Simultaneously, as an adhesive, hydrogel patches must ensure rapid and reliable adhesion to various substrates, while their re-adhesion properties after detachment and the mechanism of enhancing adhesion strength through interfacial chemistry are also crucial.[7,22,23] Based on previous researches,[24] an innovative approach of incorporating catechol-modified polyacrylic acid-dopamine (PAADA) into polyamino acid hydrogels was proposed. By utilizing the coordination of Fe^{3+}, Janus hydrogel patches were achieved. Specifically, Fe^{3+} bound to the carboxylic groups in polyamino acids and catechol groups in PAADA, forming a secondary network of coordination bonds. These sacrificial bonds significantly promoted the mechanical strength of the hydrogel patches. On the other

[a]*School of Chemistry and Chemical Engineering, Shanghai Jiao Tong University, Shanghai 200240, China. E-mail: xlwang@sjtu.edu.cn*

[b]*Department of Arthroscopic Surgery, Shanghai Jiao Tong University Affiliated Sixth People's Hospital, Shanghai 200233, China. E-mail: 0530061@fudan.edu.cn*

hand, the mussel-inspired catechol groups, as adhesive functional groups, can form abundant interactions with various substrate surfaces, therefore enhancing the adhesion effect. Notably, the PAADA on the adhesive side, unconstrained by the coordination of Fe^{3+}, possessed the ability to penetrate into soft substrates like hydrogels and biological tissues, to establish topological entanglements. These unique properties collectively endowed the hydrogel patches with excellent adhesive performance, relying on not only non-covalent hydrogen bonds for basic adhesion strength, but also stronger interfacial interactions and topological connection to elevate the adhesion interface strength to new heights.

In this work, a Janus hydrogel patch poly(*N*-acryloyl aspartic acid-*N*-acryloyl glutamic acid)/polyacrylic acid-dopamine (P(AAsp-AGlu)/PAADA) was facilely prepared using naturally-derived aspartic acid, glutamic acid, and dopamine *via* ultraviolet curing. By briefly contacting with filter paper impregnated with $FeCl_3$ solution, the hydrogel patch was endowed with excellent mechanical strength, which is about 410 kPa and presented different characteristics on each surface. Moreover, based on our previous work,[25,26] the adhesive ability of the hydrogel patch was further enhanced by combining topological stitching adhesion strategy and catechol surface chemistry, ensuring extremely low adhesion on the non-adhesive side, effectively avoiding undesired secondary adhesion while reserving the adhesive side. Besides, this Janus hydrogel patch shows high adhesion energy (about 450 J m^{-2}) after 5 adhesion cycles, which is prominent than other hydrogel adhesives.[27,28] To conclude, a hydrogel patch with robust and stable mechanical properties, universal and reversible adhesion capability was successfully developed, which perfectly meets the needs of simple operation in practical applications.

2. Results and discussion

2.1. Synthesis and characterization of PAAsp/PAADA and PAGlu/PAADA Janus hydrogels

The monomers, *N*-acryloyl aspartic acid (AAsp) and *N*-acryloyl glutamic acid (AGlu), were synthesized according to the reported (Fig. 1a).[25] ^{1}H-NMR spectroscopy was used to characterize the chemical structure of products. The results (Fig. S1) closely matched the reported data, confirming the successful synthesis of the two monomers. Dopamine-modified polyacrylic acid (PAADA) was synthesized *via* known methods.[26] Subsequently, the monomers were mixed with PAADA and UV-cured, followed by contacting a filter paper that had absorbed $FeCl_3$ solution to afford the Janus hydrogel patches (Fig. 1b). Scanning Electron Microscopy (SEM) and Energy Dispersive X-ray Spectroscopy (EDS) were utilized to characterize both sides of the lyophilized P(AAsp-AGlu)/PAADA Janus hydrogel. As illustrated in Fig. S2, the two sides of the Janus hydrogel exhibited distinctly different morphological characteristics: the adhesive surface remains relatively smooth; while the non-adhesive surface, after contacting $FeCl_3$ solution and coordinated with Fe^{3+}, displayed a rough surface. The EDS scatter Graph corroborates this observation, with almost no detectable Fe element on the adhesive surface and a significant amount of Fe distribution on the non-adhesive surface.

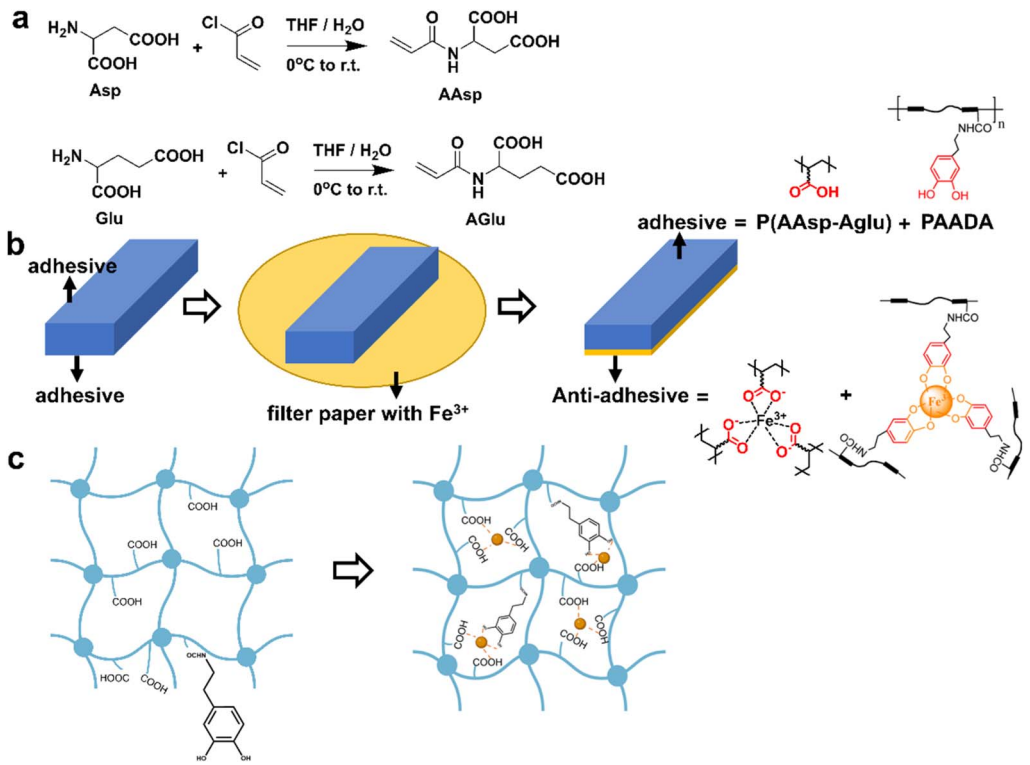

Fig. 1 Fabrication of the Janus hydrogel. (a) Synthetic procedure of AAsp and AGlu. (b) Schematic diagram of the preparation procedure of the Janus hydrogel. (c) Schematic diagram of the internal interaction of the Janus hydrogel.

The effect of solid content on the mechanical properties of hydrogel was firstly investigated. Fig. S3a illustrates the tensile strength of the PAAsp hydrogels with different solid contents. The results indicated that the single-network hydrogels exhibited relatively weak strength, with a maximum tensile strength around 80 kPa. Subsequently, the effect of the crosslinking agent methylenebisacrylamide (MBAA) on the strength of the hydrogel network was investigated. As shown in Fig. S3b, the introduction of 1 wt% MBAA significantly enhanced the strength of the hydrogels. Excessive MBAA led to a slight increase in tensile strength but a sharp decrease in strain at break of the hydrogels.

To further enhance the cohesive strength of the hydrogel, mussel-inspired PAADA was introduced into the PAAsp hydrogel precursor solution, and a PAAsp/PAADA composite hydrogel was successfully fabricated. After coordination with Fe^{3+} on one side, a PAAsp/PAADA Janus hydrogel with multiple properties was prepared. As shown in Fig. 1c, since one side of the Janus hydrogel was not exposed to Fe^{3+}, a large amount of carboxyl and catechol groups remained on the PAAsp and PAADA polymer chains, ensuring this side with excellent adhesive capabilities. On the contrary, the other side of the hydrogel lost its adhesive properties because of the coordination interaction of carboxyl and catechol groups with Fe^{3+}. Consequently, the hydrogel exhibited distinct properties on each side, and was named PAAsp/PAADA Janus hydrogel. Meanwhile, *via* the penetration of Fe^{3+} from the hydrogel surface to the interior, coordination with carboxyl and catechol groups within the hydrogel was established. The coordination interactions not only increased the crosslinking density of the hydrogel but also set up an effective stress dissipation mechanism between the covalently bonded main chains of PAAsp and PAADA. When the hydrogel undergoes deformation or damage, the dissociation of the coordination interactions efficiently dissipates energy. Therefore, the coordination of carboxyl and catechol groups with Fe^{3+} constituted the secondary network of the PAAsp/PAADA Janus hydrogel, which made a great contribution to enhance mechanical properties and meanwhile reserved the adhesive strength of the other side.

To explore the relationship between the coordination with Fe^{3+} of the hydrogels and their mechanical properties, the tensile behaviors of both the PAAsp/PAADA hydrogel without Fe^{3+} coordination and the PAAsp/PAADA Janus hydrogel with one side coordinated with Fe^{3+} were evaluated. For the PAAsp/PAADA hydrogel, as its solid content varied, the tensile strength fluctuated in the range of 120 to 250 kPa (Fig. 2a), while its strain at break ranged between 500 to 1500% (Fig. S5a). After coordinated with Fe^{3+} to form the Janus structure, the tensile properties of the PAAsp/PAADA hydrogel were significantly improved, with a maximum tensile strength exceeding 400 kPa (Fig. 2b). Although the introduction of Fe^{3+} increased the crosslinking density, resulting in a decrease in strain at break to below 800% (Fig. S5b). After a comprehensive comparison of the results, the mass fractions of PAAsp/PAADA at 30/10 wt% and 35/10 wt% were found to reach the ideal balance between the tensile strength and strain at break.

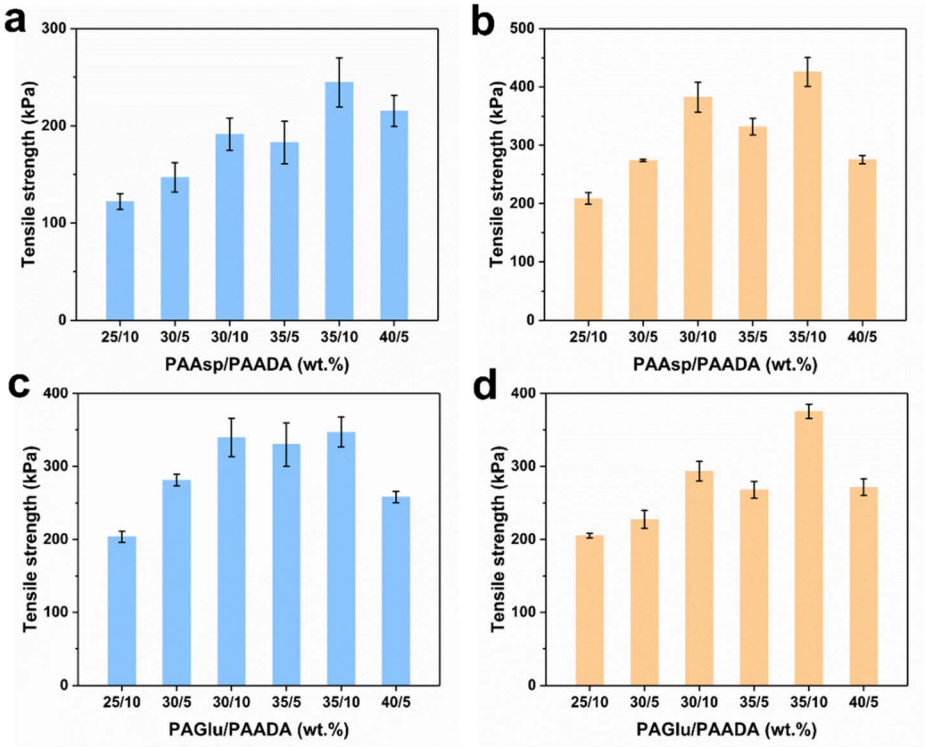

Fig. 2 Mechanical properties of PAAsp/PAADA and PAGlu/PAADA hydrogels and Janus hydrogels. (a) Tensile strength of PAAsp/PAADA hydrogels. (b) Tensile strength of PAAsp/PAADA Janus hydrogel. (c) Tensile strength of PAGlu/PAADA hydrogels. (d) Tensile strength of PAGlu/PAADA Janus hydrogels.

Additionally, an attempt was made to explore the relationship between the density of Fe^{3+} concentration and hydrogel strength by varying the concentration of $FeCl_3$ solution used to soak the filter paper (Fig. S4). Results demonstrated under the same contact time (10 s), the strength of the hydrogel increased with the increasing Fe^{3+} concentration (0.01–1 wt%).

PAGlu hydrogel with the similar structure to the PAAsp hydrogel was synthesized, and its mechanical properties was measured at varied solid contents (Fig. S3c). The results indicated that the tensile strength of the PAGlu hydrogel was greater than that of PAAsp hydrogel, reaching nearly 200 kPa. Then, the mechanical properties of PAGlu/PAADA hydrogel and PAGlu/PAADA Janus hydrogel were evaluated. PAGlu/PAADA hydrogel and PAGlu/PAADA Janus hydrogel exhibited distinctively different trends compared to PAAsp/PAADA hydrogel and PAAsp/PAADA Janus hydrogel in terms of the tensile strength. Without coordination with Fe^{3+}, the PAGlu/PAADA hydrogels already demonstrated high tensile strength, with a maximum value of approximately 350 kPa (Fig. 2c), with its strain at break reaching nearly 4000% (Fig. S5c). However, when the PAGlu/PAADA hydrogel formed a Janus structure through coordination with Fe^{3+}, the enhancement was comparatively limited. Although the strain at break decreased significantly to below 1000% (Fig. S5d), the tensile strength only increased slightly to 380 kPa (Fig. 2d). This result contrasted sharply with the significant strength enhancement observed in the PAAsp/PAADA Janus hydrogel. One possible explanation is that the introduction of Fe^{3+} indeed increases the coordination density of the PAGlu/PAADA Janus hydrogel. However, due to the structural difference between AAsp and AGlu, it may lead to insufficient effective crosslinking of Fe^{3+} between PAGlu and PAADA chains. Therefore, in the PAGlu/PAADA hydrogel, Fe^{3+} failed to effectively build a secondary network structure to enhance the mechanical properties of the hydrogel. Meanwhile, the secondary network was successfully built in the PAAsp/PAADA hydrogel. This finding contributes to understanding the impact of different molecular structures on hydrogel properties.

2.2. Mechanical properties of P(AAsp-AGlu)/PAADA Janus hydrogels

Considering the respective advantages of PAAsp and PAGlu, attempt was made to combine the strengthening effect of PAAsp/PAADA hydrogel upon coordination with Fe^{3+} and the superior strain at break of PAGlu/PAADA hydrogel. A copolymerization strategy was adopted to simultaneously improve the tensile strength and strain at break of the Janus hydrogel. Based on preliminary experimental results, 30/10 wt% was chosen as the mass fraction for P(AAsp-AGlu) and PAADA to achieve a balance between tensile strength and strain at break. Characterization of the tensile properties of P(AAsp-AGlu)/PAADA hydrogel and P(AAsp-AGlu)/PAADA Janus hydrogel was performed with a gradient of 5 wt% (Fig. 3a–c). The results showed that as the AAsp/AGlu ratio gradually decreased, the tensile strength of the P(AAsp-AGlu)/PAADA hydrogel gradually increased (Fig. 3a). After complexation with Fe^{3+}, the strength of the P(AAsp-AGlu)/PAADA Janus hydrogel exhibited a trend of slight increase followed by an obvious decrease, reaching a maximum of approximately 410 kPa at an AAsp/AGlu ratio of 20/10 (Fig. 3c). Although coordination with Fe^{3+} reduced the strain at break from 4100% to 1400%, it still remained at a relatively high level (Fig. 3b). Therefore, P(AAsp-AGlu)/PAADA = (20–10)/10 wt% was determined as the optimal mass ratio for the Janus hydrogel.

Hydrogel patches are often utilized in long-term applications which involve complex mechanical environments. To evaluate the durability of the P(AAsp-AGlu)/PAADA Janus hydrogel, cyclic tensile tests were performed. The tensile stress–strain curve and load-time curve (Fig. 3d) indicated that the Janus hydrogel can maintain good mechanical stability within a 500% strain range. In addition, the stress–strain curve at 200%, 400%, 600%, and 800% strain and the corresponding energy dissipation statistics (Fig. 3e) demonstrated the hydrogel can stably maintain its mechanical properties within the range of up to 800% strain. In terms of compressibility and elasticity, the P(AAsp-AGlu)/PAADA Janus hydrogel also exhibited excellent performance. Compared to PAAsp/PAADA Janus hydrogel and PAGlu/PAADA Janus hydrogel, P(AAsp-AGlu)/PAADA Janus hydrogel exhibited higher compressive strength at 95% deformation (Fig. 3f). The compression load-time curve and stress–strain curve in Fig. 3g further confirmed the Janus hydrogel possessed excellent compressive strength and stability.

Rheological analysis was performed to measure the storage modulus G' and loss modulus G'' of hydrogels. Frequency and strain sweeps were conducted to determine the linear viscoelastic range of the P(AAsp-AGlu)/PAADA Janus hydrogel. As shown in Fig. S6, within the tested range (0.01–10 Hz, 0.01–20% strain), the G' of the hydrogel was always larger than G'', indicating that the hydrogel was in a solid gel state and possessed stability.

In Fig. 3h, the mechanical properties of PAAsp/PAADA Janus hydrogel, PAGlu/PAADA Janus hydrogel, and P(AAsp-AGlu)/PAADA Janus hydrogel in terms of tensile strength, strain at break, Young's modulus, toughness, and energy dissipation were comprehensively summarized and compared. The copolymerized P(AAsp-AGlu)/PAADA Janus hydrogel exhibited significant advantages in terms of strain at break, toughness, and energy dissipation, giving it obvious advantages in practical applications. Its relatively low Young's modulus is mainly attributed to its strain at break which was more than twice that of the other two groups, making the hydrogel highly advantageous in scenarios requiring high flexibility due to its excellent mechanical properties.

2.3. Adhesion of P(AAsp-AGlu)/PAADA Janus hydrogels patch

The P(AAsp-AGlu)/PAADA Janus hydrogel contains abundant carboxyl and catechol moieties in its polymer chains, and these functional groups endow it with excellent adhesive properties. It was found that the P(AAsp-AGlu)/PAADA hydrogel exhibited strong adhesion to various materials, including inorganic materials (glass, Fe, Al, Cu, Ti), polymer materials (PVC, PMMA, PEEK), as well as biomaterials (wood and bone), and. With just

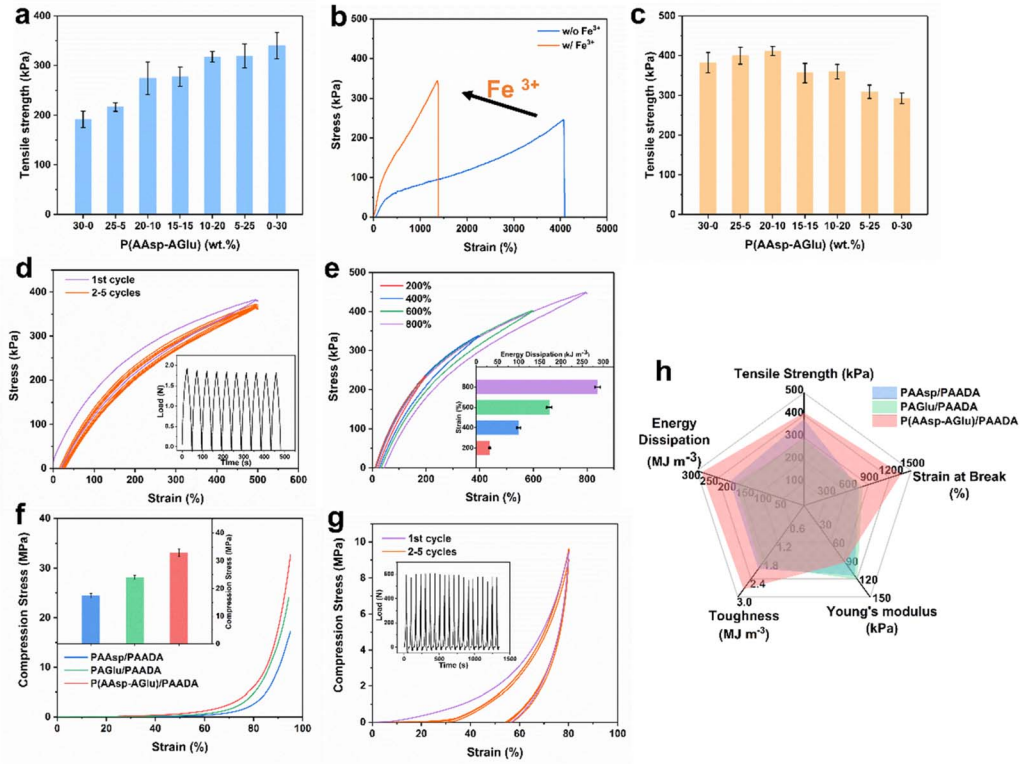

Fig. 3 Mechanical properties of P(AAsp-AGlu)/PAADA Janus hydrogels. (a) Tensile strength of P(AAsp-AGlu)/PAADA hydrogels at different mass fractions of Aasp and AGlu. (b) Tensile stress–strain curve of hydrogel with P(AAsp-AGlu)/PAADA = (20–10)/10 wt% with Fe^{3+} and without Fe^{3+}. (c) Tensile strength of P(AAsp-AGlu)/PAADA Janus hydrogels at different mass fractions of Aasp and AGlu. (d) Cyclic tensile stress–strain curve of P(AAsp-AGlu)/PAADA Janus hydrogel under 500% strain (insert is the corresponding load-time curve). (e) Tensile stress–strain curve of P(AAsp-AGlu)/PAADA Janus hydrogel under different strains (insert is the corresponding energy dissipation). (f) Compressive stress–strain curve of the three hydrogels (insert is the corresponding compression strength). (g) Cyclic compressive stress–strain curve of P(AAsp-AGlu)/PAADA Janus hydrogel (insert is the corresponding load-time curve). (h) Comparison of PAAsp/PAADA Janus hydrogel, PAGlu/PAADA Janus hydrogel and P(AAsp-AGlu)/PAADA Janus hydrogel in terms of tensile strength, elongation at break, Young's modulus, toughness and energy dissipation.

a slight press of finger, the hydrogel can form a strong adhesion to the surface of these materials in a very short time (Fig. 4a).

To further quantify the adhesive strength of the P(AAsp-AGlu)/PAADA Janus hydrogel, 90° peeling test was performed. The results are shown in Fig. 4b. The adhesive energies of the hydrogel to the aforementioned materials were mostly in the range of 400 to 500 J m^{-2} on the adhesive surface without coordination with Fe^{3+}. In particular, the adhesive energies to aluminum, glass, and bone were especially prominent, reaching over 550 J m^{-2}. Plastic substrate PVC exhibited the lowest adhesive energy, which still reached 330 J m^{-2}. Meanwhile, the adhesive energy of the non-adhesive surface with Fe^{3+} was evaluated, and the results indicated the adhesive energies to all materials were below 100 J m^{-2}, owing to the Janus structure.

The effect of Fe^{3+} on adhesive energy was further investigated. The P(AAsp-AGlu)/PAADA Janus hydrogel was brought into contact with a filter paper soaked in $FeCl_3$ solutions of different concentrations. 180° peeling test was performed and polymethacrylamide (PAAm)hydrogel without reactive functional groups was used as the adherend. Samples with no Fe^{3+} served as control. As shown in Fig. 4c, even trace amounts of Fe^{3+} can obviously reduce adhesive energy. 0.01 wt% $FeCl_3$ solution decreased the adhesive energy to approximately 120 J m^{-2}; as the concentration increased, the adhesive energy further dropped below 50 J m^{-2}. The sensitivity to Fe^{3+} of P(AAsp-AGlu)/PAADA makes it suitable for most circumstances, since only a small amount of Fe^{3+} can achieve the Janus structure of the hydrogel.

Furthermore, the kinetics of the adhesion was investigated. As illustrated in Fig. 4d, within just 10 seconds after contact, the adhesive energy rapidly reached approximately 340 J m^{-2}, demonstrating excellent instantaneous adhesive strength of the P(AAsp-AGlu)/PAADA Janus hydrogel. As PAADA on the adhesive surface of the hydrogel gradually penetrated into PAAm and formed effective entanglements with the network, the adhesive energy further increased to over 550 J m^{-2}. The result indicated in addition to the interfacial interactions of carboxyl and catechol groups, the topological stitching strategy also played a crucial role in enhancing the adhesive properties of the hydrogel with soft adherends. To investigate the impact of the stitching-bonding topological adhesion strategy on adhesion strength, PAAm hydrogels containing $NaIO_4$ were prepared as adherends to promote the formation of topological entanglement as shown in Fig. S7. Meanwhile, adhesion strength tests were conducted using a Janus hydrogel with its adhesive surface treated with $NaIO_4$ as a control. The results indicated the

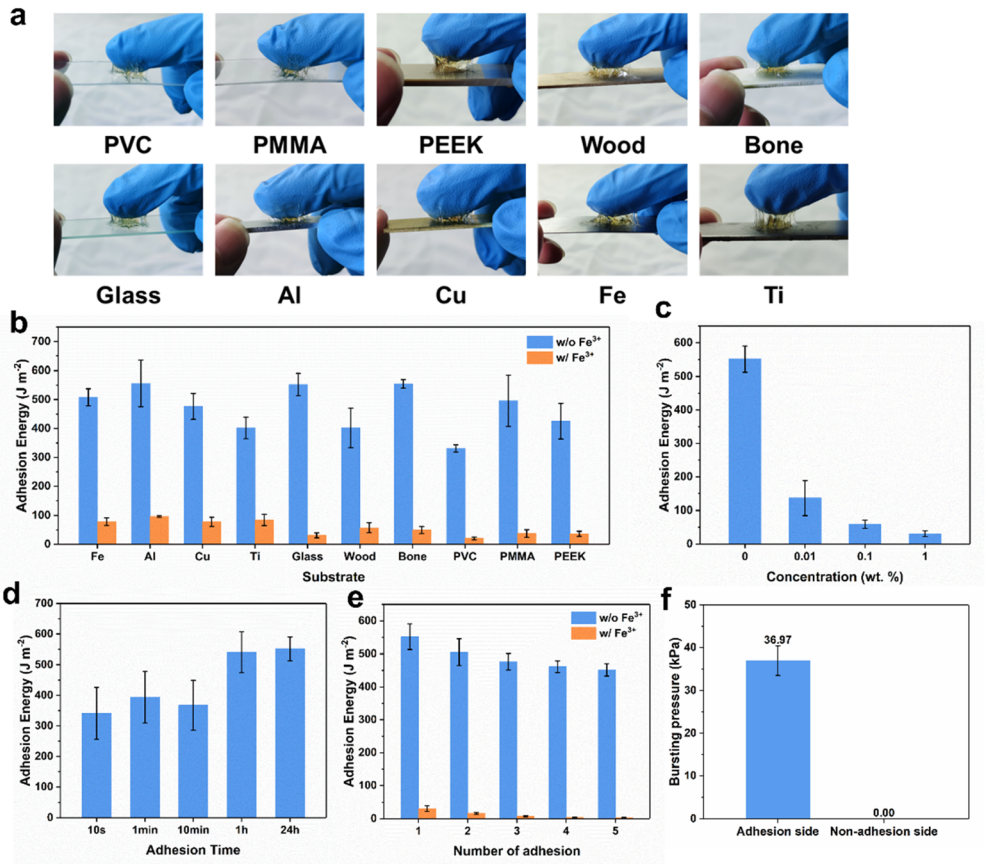

Fig. 4 Adhesion of P(AAsp-AGlu)/PAADA Janus hydrogels patch. (a) Photos of P(AAsp-AGlu)/PAADA hydrogel adhered to various substrates. (b) Adhesion energies of the adhesive surface and non-adhesive surface of P(AAsp-AGlu)/PAADA Janus hydrogel patches to various substrates. (c) Adhesion energy at different $FeCl_3$ concentrations. (d) Adhesion energy with different adhesion time. (e) Adhesion energy at different numbers of adhesion. (f) Bursting pressure of the Janus hydrogel.

adhesion energy of the non-stitching control group was only about half of that of the stitching group. Moreover, promoting entanglement *via* $NaIO_4$ treatment enhanced the adhesion energy of the hydrogel compared to the case without oxidant (dashed line). The findings demonstrated the effectiveness of the stitching-bonding strategy in improving the adhesion of hydrogel.

The repeatability of hydrogel adhesion is crucial for the hydrogel patch in practical applications. Therefore, the *in situ* repeat adhesion energy of the P(AAsp-AGlu)/PAADA Janus hydrogel after detachment was evaluated. After each detachment, the hydrogel was immediately re-adhered to the adherend and kept for 1 hour before conducting another peeling test. This process was repeated multiple times (Fig. 4e). The results showed that within five cycles, the adhesive energy of the hydrogel decreased by only about 20%, demonstrating fine repeat adhesion performance of the Janus hydrogel. Meanwhile, the non-adhesive surface exhibited consistently low adhesive energies, proving the stability of Fe^{3+} coordination.

Finally, the capacity of pressure tolerance of the P(AAsp-AGlu)/PAADA Janus hydrogel patch to biological tissues was evaluated *via* bursting pressure testing. As shown in Fig. 4f, the bursting pressure of the adhesive surface of the hydrogel to bovine arterial vessel was up to 37 kPa, far exceeding the normal blood pressure (around 16 kPa). The result suggested the P(AAsp-AGlu)/PAADA Janus hydrogel having potential capability as hemostatic materials. Meanwhile, the bursting pressure of the non-adhesive surface was nearly zero, further verifying the effectiveness of the Janus structure in preventing tissue adhesion.

2.4. Biocompatibility of the Janus hydrogels

Biocompatibility is crucial for the Janus hydrogel patches in daily use. To evaluate the cell viability of P(AAsp-AGlu)/PAADA Janus hydrogel, live/dead staining and MTT assays were employed. PAAsp/PAADA Janus hydrogel and PAGlu/PAADA Janus hydrogel served as control groups. In the live/dead staining assay, green fluorescence and red fluorescence were used to identify live and dead cells, respectively. As shown in Fig. 5a, almost no red fluorescence was observed in the groups cultured with hydrogel extracts, indicating fine cell viability of the hydrogels. Additionally, HUVEC cells exhibited consistent proliferation trends, cell morphology, and density in the experiment and control groups.

Additionally, MTT assay was conducted to assess the cytotoxicity of the P(AAsp-AGlu)/PAADA Janus hydrogel. Results

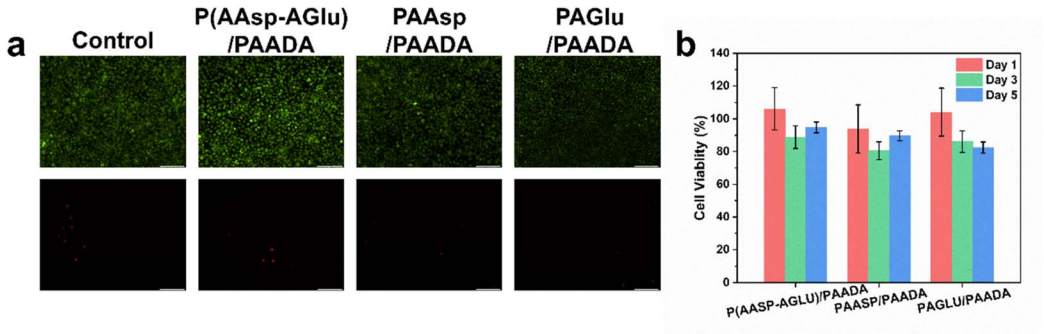

Fig. 5 Biocompatibility of the Janus hydrogels. (a) Live/dead staining photos. (b) Cell viability of the Janus hydrogels.

revealed that after culturing in hydrogel extracts at a concentration of 50 mg mL^{-1} for 1, 3, and 5 days, the viability of HUVEC cells remained above 80% of the control group, with the P(AAsp-AGlu)/PAADA Janus hydrogel group exhibiting cell viability of over 90% (Fig. 5b). Based on these findings, the safety of P(AAsp-AGlu)/PAADA Janus hydrogel for biological applications was successfully verified.

3. Conclusion

To summarize, a Janus hydrogel with two distinct sides were successfully fabricated by contacting one side of the hydrogel with a filter paper soaked in $FeCl_3$ solution, the coordination of Fe^{3+} occurred on the side, selectively eliminating its adhesive properties. Utilizing the coordination with Fe^{3+}, a strong secondary network was constructed within the hydrogel, which significantly enhanced the mechanical properties of the hydrogel, making it more suitable for direct and convenient application as a patch in various scenarios without the need for additional materials. Through interfacial adhesion of carboxyl and catechol groups, as well as the topological stitching strategy of PAADA, strong and durable adhesion to various adherends was achieved. Meanwhile, the characteristics of Janus hydrogel made its non-adhesive side extremely non-adhesive, effectively avoiding unnecessary secondary adhesion. In addition, the hydrogel exhibited good biocompatibility, providing potential for its application in fields such as wound dressing and wearable devices.

4. Materials and methods

4.1. Materials

L-Aspartic acid (Asp, Shanghai Macklin Biochemical Technology Co., Ltd), L-glutamic acid (Glu, Shanghai Macklin Biochemical Technology Co., Ltd), acryloyl chloride (Shanghai Aladdin Reagent Co., Ltd), ferric chloride hexahydrate (Shanghai Titan Scientific Co., Ltd), sodium hydroxide (Shanghai Macklin Biochemical Technology Co., Ltd), tetrahydrofuran (THF, Shanghai Macklin Biochemical Technology Co., Ltd), anhydrous ethyl ether (Sinopharm Chemical Reagent Co., Ltd), ethyl acetate (Shanghai Macklin Biochemical Technology Co., Ltd), *N*-hexane (Sinopharm Chemical Reagent Co., Ltd), *N*,*N*′-methylenebisacrylamide (MBAA, Shanghai Titan Scientific Co., Ltd), 2-hydroxy-4′-(2-hydroxyethoxy)-2-methylpropiophenone (I2959, Shanghai Titan Scientific Co., Ltd), acrylamide (AAm, Adamas-Beta), poly(acrylic acid) (PAA, 25 wt% aqueous solution, Mw = 240 000, J&K Scientific), dopamine hydrochloride (DA·HCl, InnoChem), 1-ethyl-3-(3-dimethylaminopropyl) carbodiimide hydrochloride (EDC·HCl, Adamas-Beta), *N*-hydroxysuccinimide (NHS, Adamas-Beta), 2-(*N*-morpholino)ethanesulfonic acid (MES, BidePharma) were used as received without further purification. Aluminum (Al), stainless steel (Fe), copper (Cu), titanium (Ti), polyvinyl chloride (PVC), polymethylmethacrylate (PMMA), polyether-ether-ketone (PEEK), glass, wood, and bovine bone were purchased from commercial market. Materials used as representative adherends were cut into the size of 75 mm × 25 mm or 75 mm × 30 mm. Before experiment, the surfaces of metal adherends (Fe, Al, Cu, Ti) were polished by sandpaper. All adherends were cleaned with water and ethanol, then dried at 25 °C for 1 hour.

4.2. Methods

4.2.1. Synthesis of *N*-acryloyl aspartic acid (AAsp). AAsp was synthesized according to the method reported in the literature.[24] Aspartic acid (42 g) and sodium hydroxide (38 g) were dissolved in 300 mL of deionized water and stirred in an ice bath. Subsequently, a 60 mL tetrahydrofuran solution containing 25 g of acryloyl chloride was added dropwise. The reaction was further stirred at room temperature for 5 hours. During the reaction, the pH was monitored and adjusted to maintain it between 7–8. Afterward, the pH of the mixture was adjusted to 12 with a NaOH solution, followed by washing with anhydrous ether to remove THF. The pH was then adjusted to 2 with concentrated HCl, and the aqueous phase was extracted three times with ethyl acetate. The combined organic layer was dried over anhydrous sodium sulfate, filtered, concentrated by rotary evaporation, and precipitated in *n*-hexane. The collected product was dried under vacuum to afford a white solid with a yield of approximately 12%.

N-Acryloyl glutamic acid (AGlu) was synthesized using the same method, affording a light yellow liquid with a yield of approximately 15%.

4.2.2. Synthesis of poly(acrylic acid)-dopamine (PAADA). PAADA was synthesized according to the method reported in the literature.[25,29] MES (5.85 g, 30 mmol) and NaCl (0.876 g, 15

mmol) were dissolved in deionized water (300 mL), followed by adding 5% NaOH solution to adjusted pH to 5.10 (Mettler Toledo pH meter, FE20). PAA (8.8 g, 25 wt% aqueous solution), EDC·HCl (1.92 g, 10 mmol) and NHS (1.15 g, 10 mmol) were added into the buffer solution and stirred at 60 °C under nitrogen until the solution became transparent. Then DA·HCl (9.48 g, 50 mmol) was added and reacted for 24 h. The reaction mixture was dialyzed to remove excess dopamine and lyophilized to afford PAADA.

4.2.3. Preparation of poly(*N*-acryloyl aspartic acid) (PAAsp) hydrogel. AAsp was dissolved in a certain proportion in deionized water, followed by the addition of MBAA (with a mass ratio of MBAA to Asp of 0.01 : 1) and I2959 (with a mass ratio of I2959 to AAsp of 0.01 : 1) as the crosslinker and photoinitiator, respectively. Subsequently, the precursor solution was poured into a mold consisting of two quartz plates separated by a 2 mm thick silicone spacer, with the backlight side lined with release paper for easy removal. The solution was then cured under 365 nm UV light for 30 minutes. The PAAsp hydrogel was prepared with dimensions of 60 mm × 10 mm × 2 mm.

Poly(*N*-acryloyl glutamic acid) (PAGlu) hydrogel was prepared using the same method.

4.2.4. Preparation of poly(*N*-acryloyl aspartic acid)/polyacrylic acid-dopamine (PAAsp/PAADA) hydrogel. AAsp and PAADA were dissolved in deionized water at a certain ratio, and MBAA (mass ratio of MBAA to Asp of 0.01 : 1) and I2959 (mass ratio of I2959 to AAsp of 0.01 : 1) were added as crosslinker and photoinitiator. The precursor solution was then poured into a mold composed of two quartz plates separated by a 2 mm thick silicone spacer and cured under 365 nm UV light for 30 minutes. The backlit side was lined with release paper for easy removal. The PAAsp/PAADA hydrogel was prepared with dimensions of 60 mm × 10 mm × 2 mm.

The poly(*N*-acryloyl glutamic acid)/dopamine polyacrylic acid (PAGlu/PAADA) hydrogel was prepared using the same method.

4.2.5. Preparation of poly(*N*-acryloyl aspartic acid-*N*-acryloyl glutamic acid)/polyacrylic acid-dopamine (P(AAsp-AGlu)/PAADA) Janus hydrogel patch. AAsp, AGlu, and PAADA were dissolved in deionized water at a certain ratio, and MBAA (mass ratio of MBAA to the total mass of AAsp and AGlu of 0.01 : 1) and I2959 (mass ratio of I2959 to the total mass of AAsp and AGlu of 0.01 : 1) were added as crosslinker and photoinitiator. The precursor solution was then poured into a mold composed of two quartz plates separated by a 2 mm thick silicone spacer and cured under 365 nm UV light for 30 minutes. The backlit side was lined with release paper for easy removal. The P(AAsp-AGlu)/PAADA hydrogel was prepared with dimensions of 60 mm × 10 mm × 2 mm.

Subsequently, a filter paper soaked in a certain concentration of ferrous chloride solution was placed flat on the surface of a glass dish. The prepared P(AAsp-AGlu)/PAADA hydrogel was transferred to the glass dish using release paper. After 10 seconds of unilateral contact with the filter paper, the hydrogel was removed, resulting in the P(AAsp-AGlu)/PAADA Janus hydrogel patch.

Other Janus hydrogel patches were prepared using the same method.

4.2.6. Nuclear magnetic resonance (NMR) spectroscopy. The NMR spectra of PAA, PAADA, Alg and AlgDA were measured with a Bruker (AVANCE III HD 500, 500 MHz) NMR spectrometer at room temperature. D_2O was used as solvent.

4.2.7. Scanning electron microscope (SEM) and energy dispersive X-ray spectroscopy (EDS). SEM photos of P(AAsp-AGlu)/PAADA Janus hydrogel patch were obtained on a FEI (Nova NanoSEM 450) Field Emission SEM. EDS analyses of PEI-PAA/Alg hydrogels were performed on the same instrument.

4.2.8. Tensile test. Tensile test was conducted to measure mechanical properties of P(AAsp-AGlu)/PAADA Janus hydrogel patch using a universal testing machine (Model 43 MTS Criterion) with a 500 N load cell using the hydrogel sheets (gauge length 4 mm, width 5 mm, thickness 1 mm) as specimens at the stretching speed of 100 mm min^{-1}. Toughness was calculated from the integral of stress with strain. Each test was repeated at least 3 times and the average with standard deviation was reported.

4.2.9. Compression test. The compression performance of Janus hydrogels was evaluated through compression testing. The hydrogel samples, shaped as cylinders with a base diameter of 10 mm and a height of 5 mm, were compressed at a rate of 2 mm min^{-1} under room temperature conditions in an open environment. Each group of samples was tested at least three times to calculate the mean value and standard deviation.

4.2.10. Rheological test. The performance of P(AAsp-AGlu)/PAADA Janus hydrogel was tested using a rotational rheometer. The hydrogel samples were prepared with a diameter of 7.6 mm and a thickness of 4 mm to create the gel-PU-LDA hydrogel. Mechanical properties of the PU-LDA hydrogel were tested using a rotational rheometer at 25 °C, employing parallel plates (plate diameter = 25 mm, gap = 4 mm). The frequency was scanned from 10 Hz to 0.01 Hz under a constant strain of 0.8%. Additionally, the strain was scanned from 0 to 100% at a constant frequency of 1 Hz.

4.2.11. Peeling test. 90° peeling test was performed using a universal testing machine equipped with a 500 N load cell to evaluate the adhesive strength between the rigid adherend and the hydrogel. In representative steps, P(AAsp-AGlu)/PAADA Janus hydrogel patch (60 mm × 10 mm) was pressed onto the surface of the adherend. Then, the assembly was compressed at a constant strain of 5% for 16 h at room temperature before testing. The peeling samples were sealed in plastic bags to prevent dehydration. One end of the Janus hydrogel patch was fixed to the tensile tester, and peeling was performed at a rate of 0.5 mm s^{-1}. The rigid adherend was fixed horizontally. The peeling force was measured as a function of displacement. The adhesion energy was calculated by dividing the steady value of the peeling force by the width of the hydrogel. Each sample group was tested at least three times to calculate the mean and standard deviation.

180° peeling test was performed using PAAm hydrogel with no reactive functional groups as adherend. The backside of the hydrogel was attached to a non-stretchable 20-micron-thick polyester film using cyanoacrylate glue (Krazy glue). The other conditions were the same as 90° peeling test.

4.2.12. Burst pressure test. The pressure tolerance of the P(AAsp-AGlu)/PAADA Janus hydrogel patch was tested *via* burst

pressure test. The bovine aortic vessel was connected to a syringe and a digital pressure gauge. A 5 mm hole was created on the vessel surface, and the P(AAsp-AGlu)/PAADA Janus hydrogel patch was adhered to the punctured site. The burst pressure was tested after 5 minutes. The maximum pressure value displayed by the digital pressure gauge was recorded as the burst pressure. All experiments were repeated five times, and the mean and standard deviation were calculated.

4.2.13. *In vitro* cell viability test. The cytotoxicity of P(AAsp-AGlu)/PAADA Janus hydrogel, PAAsp/PAADA Janus hydrogel, and PAGlu/PAADA Janus hydrogel was evaluated using HUVEC cells through the MTT method. Cells were seeded in 96-well plates at a density of 5000 cells per well and cultured for 24 h in DMEM containing 10% FBS under a humidified atmosphere at 37 °C and 5% CO_2. The Janus hydrogel patches were extracted at 100 mg mL^{-1} using DMEM for 24 h. Subsequently, the culture medium was replaced with the hydrogel extract solutions and further cultured for 48 h. DMEM without hydrogel addition was set as a positive control. After incubation, 20 μL of MTT solution (1 mg mL^{-1}) was added, and the cells were further cultured for 4 h in the dark. Then, the solution was removed, and the cells were photographed using a microscope. Finally, 200 μL of DMSO was added to dissolve the formazan, and the absorbance at 490 nm was measured using a microplate reader. The relative cell viability was calculated using the formula:

$$\text{Cell viability} = (A_x - A_b)/(A_c - A_b) \times 100\%$$

where "A_x", "A_b" and "A_c" represent mean absorbance value of the sample, background and control, respectively. The sample with relative cell viability more than 75% was considered to be bio-compatible.

Further evaluation of cell proliferation was conducted through live/dead staining. L929 cells were seeded into 24-well plates at a density of 2×10^4 cells per well and cultured for 24 h in DMEM medium containing 10% FBS under standard culture conditions. The medium was replaced with the hydrogel extract (50 mg mL^{-1}), and the cells were further cultured for 1 day. Live/dead cells were stained with calcein-AM/propidium iodide dyes separately. Green (492 nm) and red (545 nm) fluorescence were observed and photographed under a fluorescence microscope.

Conflicts of interest

The authors declare no conflicts of interest.

Data availability

All relevant data are within the manuscript and SI. See DOI: https://doi.org/10.1039/d5ra04058b.

Acknowledgements

This work was financially supported by National Nature Science Foundation of China (No. 52201184) and Interdisciplinary Program of Shanghai Jiao Tong University (YG2022QN085).

References

1 G. Chen, Y. Yu, X. Wu, *et al.*, Bioinspired Multifunctional Hybrid Hydrogel Promotes Wound Healing, *Adv. Funct. Mater.*, 2018, **28**(33), 1801386.
2 J. Zhu, F. Li, X. Wang, *et al.*, Hyaluronic Acid and Polyethylene Glycol Hybrid Hydrogel Encapsulating Nanogel with Hemostasis and Sustainable Antibacterial Property for Wound Healing, *ACS Appl. Mater. Interfaces*, 2018, **10**(16), 13304–13316.
3 X. Peng, X. Xu, Y. Deng, *et al.*, Ultrafast Self-Gelling and Wet Adhesive Powder for Acute Hemostasis and Wound Healing, *Adv. Funct. Mater.*, 2021, **31**(33), 2102583.
4 M. Xie, Y. Zeng, H. Wu, *et al.*, Multifunctional carboxymethyl chitosan/oxidized dextran/sodium alginate hydrogels as dressing for hemostasis and closure of infected wounds, *Int. J. Biol. Macromol.*, 2022, **219**, 1337–1350.
5 Z. Chen, J. Yao, J. Zhao, *et al.*, Injectable wound dressing based on carboxymethyl chitosan triple-network hydrogel for effective wound antibacterial and hemostasis, *Int. J. Biol. Macromol.*, 2023, **225**, 1235–1245.
6 H. Jung, M. K. Kim, J. Y. Lee, *et al.*, Adhesive Hydrogel Patch with Enhanced Strength and Adhesiveness to Skin for Transdermal Drug Delivery, *Adv. Funct. Mater.*, 2020, **30**(42), 2004407.
7 Y. Jiang, X. Zhang, W. Zhang, *et al.*, Infant Skin Friendly Adhesive Hydrogel Patch Activated at Body Temperature for Bioelectronics Securing and Diabetic Wound Healing, *ACS Nano*, 2022, **16**(6), 8662–8676.
8 J. Liu, M. Qu, C. Wang, *et al.*, A Dual-Cross-Linked Hydrogel Patch for Promoting Diabetic Wound Healing, *Small*, 2022, **18**(17), 2106172.
9 P. Chen, W. Zhang, X. Fan, *et al.*, A polyphenol-derived redox-active and conductive nanoparticle-reinforced hydrogel with wet adhesiveness for myocardial infarction repair by simultaneously stimulating anti-inflammation and calcium homeostasis pathways, *Nano Today*, 2024, **55**, 102157.
10 Y. Cong and J. Fu, Hydrogel–Tissue Interface Interactions for Implantable Flexible Bioelectronics, *Langmuir*, 2022, **38**(38), 11503–11513.
11 J. Shin, J. S. Lee, C. Lee, *et al.*, Tissue Adhesive Catechol-Modified Hyaluronic Acid Hydrogel for Effective, Minimally Invasive Cell Therapy, *Adv. Funct. Mater.*, 2015, **25**(25), 3814–3824.
12 Z. Li, L. Liu and Y. Chen, Dual dynamically crosslinked thermosensitive hydrogel with self-fixing as a postoperative anti-adhesion barrier, *Acta Biomater.*, 2020, **110**, 119–128.
13 Q. Yu, H. Sun, L. Zhang, *et al.*, A Zwitterionic Hydrogel with Anti-Oxidative and Anti-Inflammatory Properties for the Prevention of Peritoneal Adhesion by Inhibiting Mesothelial-Mesenchymal Transition, *Adv. Healthcare Mater.*, 2023, **12**(30), 2301696.
14 Q. Wang, J. Lan, Z. Hua, *et al.*, An oriented Fe3+-regulated lignin-based hydrogel with desired softness, conductivity, stretchability, and asymmetric adhesiveness towards anti-

interference pressure sensors, *Int. J. Biol. Macromol.*, 2021, **184**, 282–288.
15 W. Liang, W. He, R. Huang, *et al.*, Peritoneum-Inspired Janus Porous Hydrogel with Anti-Deformation, Anti-Adhesion, and Pro-Healing Characteristics for Abdominal Wall Defect Treatment, *Adv. Mater.*, 2022, **34**(15), 2108992.
16 C. Cui, T. Wu, X. Chen, *et al.*, A Janus Hydrogel Wet Adhesive for Internal Tissue Repair and Anti-Postoperative Adhesion, *Adv. Funct. Mater.*, 2020, **30**(49), 2005689.
17 H. Wang, X. Yi, T. Liu, *et al.*, An Integrally Formed Janus Hydrogel for Robust Wet-Tissue Adhesive and Anti-Postoperative Adhesion, *Adv. Mater.*, 2023, **35**(23), 2300394.
18 W. Peng, C. Liu, Y. Lai, *et al.*, An Adhesive/Anti-Adhesive Janus Tissue Patch for Efficient Closure of Bleeding Tissue with Inhibited Postoperative Adhesion, *Advanced Science*, 2023, **10**(21), 2301427.
19 T. Nonoyama and J. P. Gong, Double-network hydrogel and its potential biomedical application: A review[J]. Proceedings of the Institution of Mechanical Engineers. Part H, *J. Eng. Med.*, 2015, **229**(12), 853–863.
20 Z. Jiang, Y. Li, Y. Shen, *et al.*, Robust Hydrogel Adhesive with Dual Hydrogen Bond Networks, *Molecules*, 2021, **26**(9), 2688.
21 G. Zhang, S. Chen, Z. Peng, *et al.*, Topologically Enhanced Dual-Network Hydrogels with Rapid Recovery for Low-Hysteresis, Self-Adhesive Epidemic Electronics, *ACS Appl. Mater. Interfaces*, 2021, **13**(10), 12531–12540.
22 L. Sun, J. Zhou, J. Lai, *et al.*, Novel Natural Polymer-Based Hydrogel Patches with Janus Asymmetric-Adhesion for Emergency Hemostasis and Wound Healing, *Adv. Funct. Mater.*, 2024, **34**(36), 2401030.
23 Y. Mi, Y. Niu, H. Ni, *et al.*, Gecko inspired reversible adhesion *via* quantum dots enabled photo-detachment, *Chem. Eng. J.*, 2022, **431**, 134081.
24 J. Yu, K. Xu, X. Chen, *et al.*, Highly Stretchable, Tough, Resilient, and Antifatigue Hydrogels Based on Multiple Hydrogen Bonding Interactions Formed by Phenylalanine Derivatives, *Biomacromolecules*, 2021, **22**(3), 1297–1304.
25 B. Chen, D. Zhu, Q. Li, *et al.*, Mechanically Reinforced and Injectable Universal Adhesive Based on a PEI–PAA/Alg Dual-Network Hydrogel Designed by Topological Entanglement and Catechol Chemistry, *ACS Appl. Mater. Interfaces*, 2023, **15**(51), 59826–59837.
26 B. Chen, D. Zhu, R. Zhu, *et al.*, Universal adhesion using mussel foot protein inspired hydrogel with dynamic interpenetration for topological entanglement, *Int. J. Biol. Macromol.*, 2024, **256**, 127868.
27 S. Li, L. Zhi, Q. Chen, *et al.*, Reversibly Adhesive, Anti-Swelling, and Antibacterial Hydrogels for Tooth-Extraction Wound Healing, *Adv. Healthcare Mater.*, 2024, **13**(14), 2400089.
28 G. Pan, F. Li, S. He, *et al.*, Mussel- and Barnacle Cement Proteins-Inspired Dual-Bionic Bioadhesive with Repeatable Wet-Tissue Adhesion, Multimodal Self-Healing, and Antibacterial Capability for Nonpressing Hemostasis and Promoted Wound Healing, *Adv. Funct. Mater.*, 2022, **32**(25), 2200908.
29 Y. Gao, J. Chen, X. Han, *et al.*, A Universal Strategy for Tough Adhesion of Wet Soft Material, *Adv. Funct. Mater.*, 2020, **30**(36), 2003207.